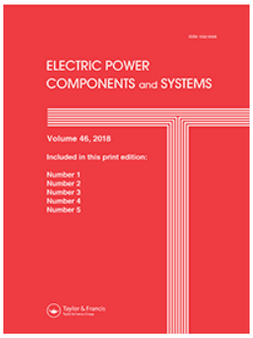

Taylor & Francis
Taylor & Francis Group

Electric Power Components and Systems

ISSN: 1532-5008 (Print) 1532-5016 (Online) Journal homepage: http://www.tandfonline.com/loi/uemp20

Multi-Domain Model of Faulty Stator Core for Thermal Effects and Losses Evaluation

Luis I. Silva, Pablo M. de la Barrera, Roberto Leidhold, Guillermo R. Bossio & Cristian H. De Angelo

To cite this article: Luis I. Silva, Pablo M. de la Barrera, Roberto Leidhold, Guillermo R. Bossio & Cristian H. De Angelo (2018) Multi-Domain Model of Faulty Stator Core for Thermal Effects and Losses Evaluation, Electric Power Components and Systems, 46:2, 187-196, DOI: 10.1080/15325008.2018.1444685

To link to this article: https://doi.org/10.1080/15325008.2018.1444685

Published online: 09 Apr 2018.

Submit your article to this journal

Article views: 25

View related articles

View Crossmark data

Full Terms & Conditions of access and use can be found at
http://www.tandfonline.com/action/journalInformation?journalCode=uemp20

Electric Power Components and Systems, 46(2):187–196, 2018
Copyright © Taylor & Francis Group, LLC
ISSN: 1532-5008 print / 1532-5016 online
DOI: 10.1080/15325008.2018.1444685

Taylor & Francis
Taylor & Francis Group

Check for updates

Multi-Domain Model of Faulty Stator Core for Thermal Effects and Losses Evaluation

Luis I. Silva,[1] Pablo M. de la Barrera,[1] Roberto Leidhold,[2]
Guillermo R. Bossio,[1] and Cristian H. De Angelo[1]
[1]Grupo de Electrónica Aplicada (GEA), Facultad de Ingeniería Universidad Nacional de Río Cuarto, Argentina
[2]Institute of Electric Power Systems, Otto-von-Guericke-Universität Magdeburg, Germany

CONTENTS

Abstract—In this work, a multi-domain model of the stator core of an electric machine is presented. Its electromagnetic behavior and the thermal dynamics are represented using Bond Graph. This approach makes apparent the topology of the machine and the energy exchange. This feature enables the model for the easy representation of faults and analysis of their consequences in the thermal/magnetic/electric domain. The proposed model is used for reproducing the behavior of the stator core during an inter-laminar insulation test. The model is capable to reproduce the thermal distribution when a fault in the stator core occurs. This contribution helps to estimate the additional iron losses due to the stator core fault based on the thermal distribution. Additionally, this methodology could help to define the proper maintenance intervention to be performed on the machine.

1. INTRODUCTION

The early detection of failures in electrical machines is gaining interest, in correlation with the growing complexity of the systems using these machines. It is worth mentioning that a machine failure often produces a system damage or outage leading to much higher costs than the replacement of the machine itself. The early detection and accurate evaluation of incipient failures, allows to repair or replace the machine in a scheduled maintenance procedure, before any damage or outage.

There are numerous methods proposed in the literature for failure detection and evaluation [1], [2]. They can be classified in offline methods, which require to take the machine out of operation (with or without disassembling [3]); and online methods, which evaluates the machine while being in operation [4]. Online methods which only evaluate the stator voltages and currents [5], [6] are, on the one hand, the most challenging. On the other hand, their implementation is simple in inverter-driven machines.

Stator core faults (SCF) are caused by inter-lamination short circuits, see Figure 1. These can propagate, because the

Keywords: electric machines, stator core faults, full test ring, multi-domain model, bond graph

Received 6 April 2016; accepted 11 February 2018

Address correspondence to Pablo M. de la Barrera, Grupo de Electrónica Aplicada (GEA), Facultad de Ingeniería Universidad Nacional de Río Cuarto, Argentina. E-mail: pbarrera@ieee.org

Color versions of one or more of the figures in the article can be found online at www.tandfonline.com/uemp.

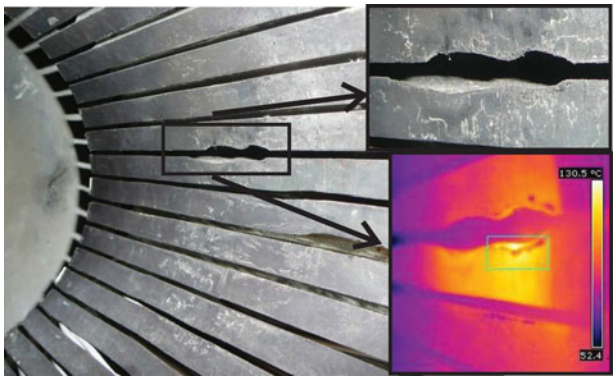

FIGURE 1. Real stator core fault in a 294 kW induction machine.

localized heating due to the eddy currents through the shorted lamination produces further damage in the inter-lamination insulation or even melt laminations together [7]. Stator core failures are less frequent than other failure types. However, they can also produce important damage and they are more difficult to detect in an early stage [2]. Only a few online methods have been reported until now, namely: gas particulate core condition monitors [1], external flux density sensor [7] and signal injection for small machines [8]. For further development of these detection methods, an adequate model of the machine for representing inter-lamination short circuit effects is crucial.

In [9], a model is proposed to evaluate the increase of losses in the shorted laminations. This model analyzes the local phenomena disregarding its interaction with the whole machine. An approach to estimate the current through inter-lamination contact in a transformer core is proposed in [10]. By using a permeance network, the impedance of a coil around the faulty core is determined. Two-dimensional (2D) and three-dimensional (3D) analytical models are presented in [3] to evaluate the core fault currents and how they are detected by the magnetic probes as used in offline methods. In [11], a 3D finite element model (FEM) is implemented and validated with an offline detection method considering just a portion of the machine core. The 3D FEM are computational intensive thus they are not adequate for the design (synthesis) of online fault detection methods. Electric machine models which consider the thermal behavior are presented in [12] without experimental validation. Moreover, such proposals are not oriented to a specific SCF test.

The aim of the present article is to develop a multi-domain model including inter-lamination short circuits. The proposed model supports the analysis of the electromagnetic and thermal implications of the fault, leading to evaluate the severity of the stator core faults.

The model proposed in this article is based on a magnetic equivalent circuit (MEC) [13] which is a halfway approach between lumped parameters [14] and those finite element models proposed in [15]. The model is represented using Bond Graph (BG) which is best suited to represent multi-domain systems, as stated in [16]. Additionally, it provides a direct correspondence with the topology of the system thus different faults can be easily introduced.

This model also gives us new important information about the temperature evolution in order to find new indicators for early detection of SCF. This information is applicable to both offline and online experimental tests. In addition, the utilization of this methodology would help to define the proper moment for repairing and the maintenance intervention to be performed on the machine.

2. ELECTROMAGNETIC MODELING

In the traditional MEC method the magnetomotive force (MMF denoted by $\mathcal{F}$) is considered analogous to voltage, while magnetic flux (Φ) is analogous to electric current. Reluctance ($\mathcal{R}$) is then equivalent to electric resistance and Hopkinson's law ($\mathcal{F} = \mathcal{R}\Phi$) is a counterpart to Ohm's law. Although these concepts have been widely used, from the energetic point of view, they are not satisfactory. Actually, the reluctance behaves as a magnetic-energy storage element and not as a dissipative element [17]. This fact is easy to understand if the *effort* and *flow* variables are analyzed [18]. These variables could be obtained from any complex mathematical expression such as a matrix, vector or phasor. When modeling a system, the *effort* and *flow* are usually chosen such that their product is power. Table 1 shows these variables for different domains and the product of their units. It is thus evident that in the magnetic domain, with the traditional approach, this product results in energy unit.

An alternative analogy between magnetic and electric domains is proposed in [19], where $\mathcal{F}$ is maintained as the *effort* variable, but the *flow* variable is the rate-of-change of Φ ($\frac{d}{dt}\Phi$). With this alternative analogy, the *effort-flow* product is power ((A) (Wb/s) = (W)) and the permeance ($\mathcal{P} = \frac{1}{\mathcal{R}}$) is

Domain	Effort (unit)	Flow (unit)	Effort Flow Product
Thermal	Temp. (K)	Entropy flow ($\frac{J}{Ks}$)	(K $\frac{J}{Ks}$) = (W)
Electric	Voltage (V)	Current (A)	(V A) = (W)
Mechanic	Force (N)	Velocity ($\frac{m}{s}$)	(N $\frac{m}{s}$) = (W)
Magnetic	MMF (A)	Mag. flux (Wb)	(A Wb) = (J)

TABLE 1. *Effort* and *Flow* variables for different domains.

equivalent to electric capacitance. It is related with the other variables by: $\frac{d}{dt}\Phi = \mathcal{P}\frac{d}{dt}\mathcal{F}$.

2.1. MEC Model

The SCF occurs when the inter-laminar insulation deteriorates producing an increase of eddy currents that circulate along the key bars and the laminations affected by the fault, see Figure 2(a). Eddy currents that circulate under non-faulty operation are represented with the current loop i_{ed} circulating along the total perimeter of the core section, see Figures 2(b) and (c). The model includes an external test coil used to perform the inter-laminar insulation test [20], that consists in generating a flux in the core. Figure 2(b) shows the idealized physical system that represents the arrangement of the test. For this analysis, all flux from induction and fault is assumed to remain circumferential within the laminations. The test coil, with N_i turns and resistance R_i, is fed by a voltage source (V_i). In the same figure, the SCF is modeled as a current loop i_f embedded in the core. In this model, the severity of the SCF can be varied changing the width of the current loop.

The criteria adopted to obtain the MEC model consists on considering as a single magnetic element those portion of material, where the magnetic flux is colinear and the permeability is constant. The resulting model is depicted in Figure 2(c). Based on the electromagnetic representation of Figure 2(c), the equations of the MEC can be obtained, by inspection from Figure 2(c), as follows:

$$a_2 - f_2(\Phi_2) = 0 \tag{1}$$

$$a_2 - \mathcal{F}_f - f_f(\Phi_f) = 0 \tag{2}$$

$$a_2 - \mathcal{F}_i - \mathcal{F}_{ed} + f_i(\Phi_i) = 0 \tag{3}$$

$$f_{12}(\Phi_i) + f_{41}(\Phi_i) + f_{34}(\Phi_i) = f_i(\Phi_i) \tag{4}$$

Here, a_k, with k =1, 2, 3 and 4, represents the magnetic potential in the nodes (a_3 was chosen as the reference magnetic node). Subscripts i, ed, and f represent variables associated with input, eddy currents, and fault circuits, respectively. More complex analytical models for computing eddy currents are presented in [21].

In order to consider the B–H curve of the material, all permeances of the MEC were modeled as non-linear [22]. Figure 3 shows the B–H curve of the core material obtained experimentally and its approximation (dashed line) of the

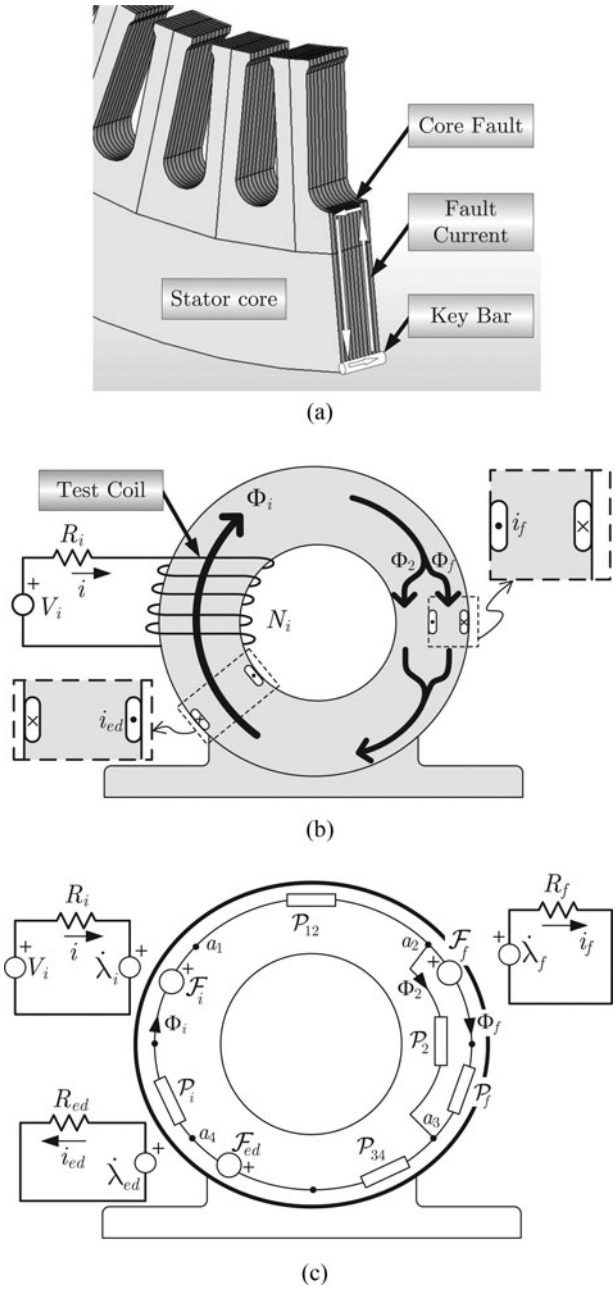

FIGURE 2. (a) Stator core fault, (b) ideal system, and (c) MEC model.

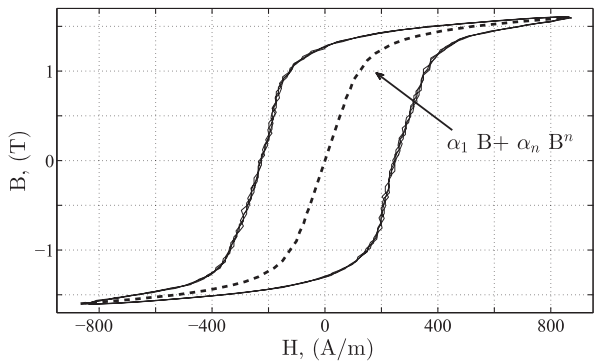

FIGURE 3. Experimental B–H curve and an approximation without hysteresis.

curve without hysteresis. The model used to fit the B–H curve is given by [23]:

$$f(\Phi) = \frac{l\alpha_1}{S}\Phi + \frac{l\alpha_n}{S^n}\Phi^n + \frac{l\beta_1}{S}\frac{d}{dt}\Phi + \frac{l\beta_m}{S^m}\left(\frac{d}{dt}\Phi\right)^m \quad (5)$$

The first and second terms of (5) represent the non-linear saturation of the material, see the dashed line in Figure 3, while the third and fourth terms represent the magnetic hysteresis. The constants of (5) (α_1, α_n, β_1, and β_m) are adjusted from the experimental B–H curve. Parameters l and S are the magnetic path length and the cross-section of the magnetic tube, respectively. For the magnetic tubes affected by the fault the cross-sections (S_2 and S_f) are given by:

$$\left.\begin{array}{l} S_2 = (1-\delta)S_t \\ S_f = \delta S_t \end{array}\right\} \rightarrow 0 \leq \delta \leq 1 \quad (6)$$

where S_t is the total cross-section of the core in the faulty region and δ is the severity factor. δ is defined as the proportion of axial length of the motor which is faulted, namely:

$\delta = 0 \rightarrow$ healthy operation

$\delta = 1 \rightarrow$ complete inter-laminar short circuit.

The electric and magnetic domains are related by the following equations:

$$\begin{array}{l} \mathcal{F}_i = N_i i \;\; ; \;\; \mathcal{F}_f = N_f i_f \;\; ; \;\; \mathcal{F}_{\text{ed}} = N_{\text{ed}} i_{\text{ed}} \\ \lambda_i = N_i \Phi_i \;\; ; \;\; \lambda_f = N_f \Phi_f \;\; ; \;\; \lambda_{\text{ed}} = N_{\text{ed}} \Phi_i \end{array} \quad (7)$$

where N_i, N_f, and N_{ed} represent the numbers of turns of the test coil, the fault loop, and eddy current loop, respectively. The dynamic equations for electric domain are obtained analyzing Figure 2(c) as:

$$\dot{\lambda}_i = \tfrac{d}{dt}\lambda_i = V_i - R_i i \,; \;\; \dot{\lambda}_f = \tfrac{d}{dt}\lambda_f = -R_f i_f \quad (8)$$

where V, i, R, and λ are voltage, current, resistance, and flux linkage, respectively.

R_f represents the equivalent resistance of the fault loop and it can be estimated by calculating the resistances of the following paths: the key bar, sheets of lamination and the fault, as it was indicated in Figure 2(a). For the simulation, it was used $R_f = [0.1123,\ 0.1401,\ 0.1680]\ \Omega$ for the following severity factors $\delta = [0.3,\ 0.65,\ 1]$.

2.2. Representation Using BG

The BG representation of the magnetic circuit is obtained from the ideal system proposed in Figure 2(c). The resulting model is depicted in Figure 4.

This model is called "*Permeance Network Model*" [24] and presents a direct correspondence with the topology of the real system. By using BG, the complete representation is obtained without resorting to any mathematical model.

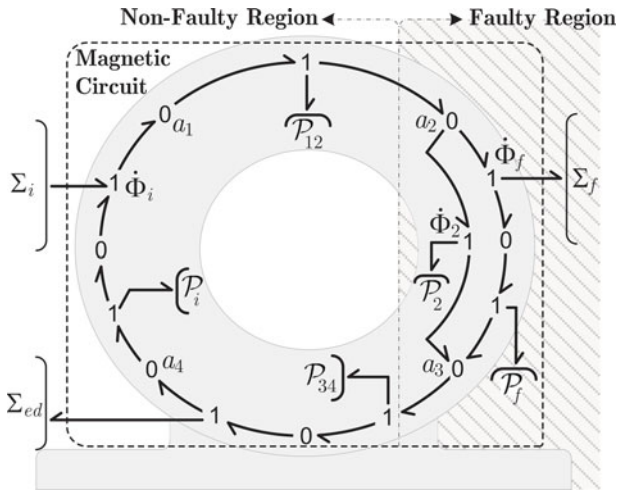

FIGURE 4. Structure of the magnetic circuit in BG.

The magnetic material is represented using a non-linear capacitor ($\mathbf{C^H}$) and a non-linear resistor ($\mathbf{R^H}$) which relates effort and flow as follows:

$$\Phi = \Phi_0 + \int_0^t f(\tau)\, d\tau$$

$$e = \mathcal{F}_1 = \frac{l\alpha_1}{S}\Phi + \frac{l\alpha_n}{S^n}\Phi^n \quad (9)$$

$$e = \mathcal{F}_2 = \frac{l\beta_1}{S}\dot{\Phi} + \frac{l\beta_m}{S^m}\dot{\Phi}^m \quad (10)$$

From (9) and (10), it can be inferred that the dynamics of this BG element is equivalent to (5). The BG representation is shown in Figure 5.

The coupling between electric and magnetic domain is represented using a gyrator element (**GY**) with constitutive relationship given by:

$$e_2 = N\, f_1 \;\; ; \;\; e_1 = N\, f_2 \quad (11)$$

where N is the number of turns, thus making the expression equivalent to (7).

The representation of the complete electromagnetic system includes the electric dynamics and its structure is simplified, by assuming $a_3 = 0$, see Figure 6.

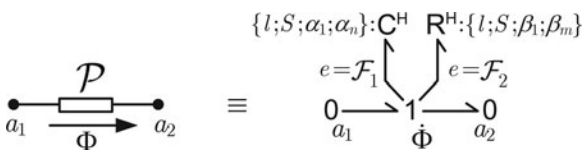

FIGURE 5. Representation of the permeance in BG.

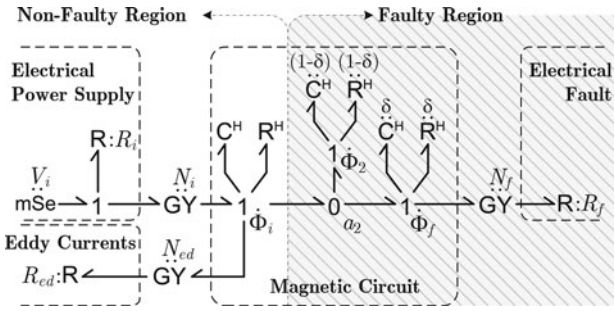

FIGURE 6. Complete electromagnetic model using BG.

3. THERMAL MODELING

Due to the negative impact of overheating on the motor life, models capable to reproduce the electromagnetic and the thermal dynamics become essential to evaluate the thermal impact of different faults. The thermal model of the system is first presented in Section 3.1 together with the modeling hypotheses. The representation using BG, based on these hypotheses, is then presented in Section 3.2

3.1. Thermal Model

The thermal model [25], [26] considers teeth and slots as independent elements, see E_3 and E_4 in Figure 7(a). To keep consistency, the external part of the stator yoke is divided into two elements (E_1 and E_2). This array of four elements is repeated 48 times which is the number of stator teeth/slots. The complete connection of these elements gives rise to a 2D thermal model of the stator core. Next, the criterion adopted to model the thermal behavior is summarized:

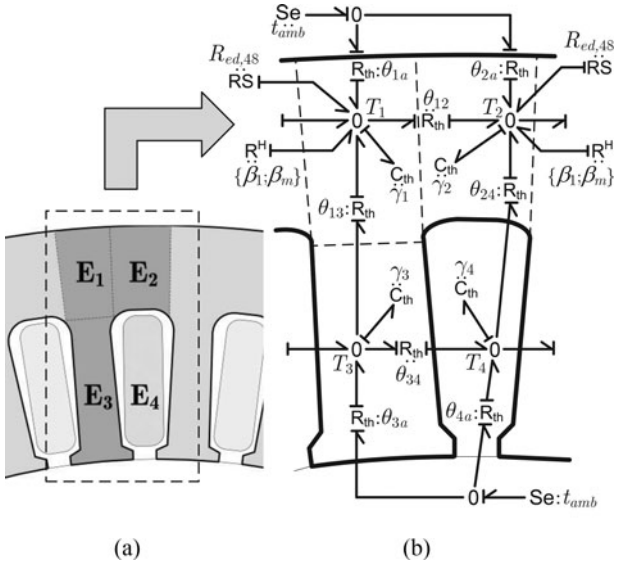

FIGURE 7. (a) Division of elements in the 2D model of the stator core, and (b) BG representation.

- E_1, E_2, E_3, and E_4 interchange heat by conduction with their neighbors and dissipate heat to the environment.
- The stator yoke (E_1 and E_2) receives the heat dissipated in R_{ed} and $\mathbf{R^H}$.
- The tooth and E_1 where the fault occurs receive the heat dissipated in R_f.
- Elements surrounded by the test coil interchange heat by conduction with it.
- Test coil is considered as a single element that receives the heat dissipated by R_i and dissipate heat toward the ambient.
- Thermal radiation is neglected.

Conduction Between Elements is produced as consequence of the temperature difference. Each element interchanges heat by conduction according to the experimental Fourier law:

$$\frac{\partial Q}{\partial t} = -\frac{A}{\rho}\frac{\partial T}{\partial x} \tag{12}$$

The rate of heat transfer ($\partial Q/\partial t$) takes place through the cross-sectional area A; ρ is the thermal resistivity between the elements. $\partial T/\partial x$ is the spatial temperature gradient. In this case:

$$\frac{\partial T}{\partial x} = \frac{\Delta T}{\Delta x} = \frac{(T_i - T_j)}{\Delta x} \tag{13}$$

where $T_{i,j}$ is the temperature of element (i, j) and Δx is the distance between the center of elements.

Dissipation Toward the Ambient takes place by conduction and convection. This process can be considered as conduction, where the thermal resistance is modulated as a function of the ventilation. In our case, there is not forced ventilation thus the resistance remains constant. The temperature on the other side of the thermal resistance is maintained equal to the ambient temperature t_{amb}.

Heat Storage is based on the first law of thermodynamics and assuming that neither phase change nor network occur in the element:

$$Q = \gamma \Delta T \tag{14}$$

where Q is the absorbed heat, γ is the heat capacity, and ΔT is the temperature variation produced in the element.

All the sources of entropy plus the incoming/outgoing entropy via conduction conform the total flow of entropy ($\dot{S}$). The rate of heat flow ($\partial Q/\partial t$) is obtained by multiplying the total flow of entropy and element temperature. Hence, (14)

can be re-written in differential form as:

$$\dot{S} = \frac{d}{dt}S = \frac{\gamma}{T}\frac{d}{dt}T \tag{15}$$

Equation (15) is used to determine the temperature evolution using total flow of entropy and the initial temperature.

3.2. Representation Using BG

The complete thermal behavior modeled in BG is presented in Figure 7(b). Here the bondgraphic generalized effort (e) represents temperature (T) and the flow (f) is the flow of entropy ($\dot{S}$).

Conduction Between Elements is represented with a thermal resistance "$\mathbf{R_{th}}$" whose relationship between primary and secondary bonds is

$$f_1\, e_1 = \frac{1}{\theta}(e_1 - e_2) \tag{16}$$

$$f_2 e_2 = f_1 e_1 \tag{17}$$

where the product $f_1\ e_1$ is the rate of heat flow ($\partial Q/\partial t$). Replacing $\theta = \rho\ \Delta x/A$ (thermal resistance), (16) becomes equivalent to (13). To model the effect of ventilation in the dissipation toward the ambient, θ is modulated. In this case, θ is constant given that no ventilation is applied. Equation (17) states that the outgoing heat from an element is totally transferred to the other.

Dissipation Toward the Ambient in BG is a special case of conduction where the thermal resistance is modulated as a function of the ventilation and the ambient temperature is fixed using a source of effort ($\mathbf{Se} = t_{\text{amb}}$).

Heat Storage is represented with a thermal capacity $\mathbf{C_{th}}$. It inherits the relationship from electric capacity but in this case the value of the capacity is inversely proportional to element temperature (i.e., $C = \gamma/e$). With this substitution, the relationship becomes equivalent to (15).

The BG representation of the 2D thermal model is finally presented in Figure 7(b). Here, subscripts 1,2,3,4 and a used in parameters refer to $\mathrm{E}_{1,2,3,4}$ and ambient, respectively. $R_{\text{ed,48}}$ refers to the portion of R_{ed} that corresponds this element.

It is worth mentioning that all parameters used in the thermal model are obtained directly from the geometry of the machine and the intrinsic parameters of materials.

3.3. Coupling the BG Electromagnetic and Thermal Models

The incoming heat produced by the dissipation on the electric resistances (R_{ed} and R_f) is modeled with a resistive source "**RS**." Relationship between primary and secondary bonds is given by:

$$e_1 = R\, f_1\ ;\ f_2 = f_1 e_1/e_2. \tag{18}$$

Primary bond (indicated with subscript 1) belongs to the electric domain and has free causality. Secondary bond (subscript 2) enters the thermal model as a source of entropy.

In order to contemplate the power dissipated in the $\mathbf{R^H}$ that represents the magnetic hysteresis, this element is redefined as a bi-port element (magnetic resistive source). Primary bond belongs to the magnetic domain and secondary bond enters the thermal model as a source of entropy. Its constitutive relationship is given by:

$$e_1 = \frac{l\beta_1}{S} f_1 + \frac{l\beta_m}{S^m} f_1^m \tag{19}$$

$$f_2 e_2 = f_1 e_1 \tag{20}$$

where (19) is equivalent to (10) and (20) indicates that all the dissipated magnetic energy is transformed into heat.

4. OBTAINED RESULTS

The proposed BG model was implemented in 20SIM and it was used to obtain the simulation results. Experimental results were obtained by implementing the loop test in the stator core of a 5.5 kW machine as proposed in [27]. The first part is devoted to validate the proposed model. After adjusting and tuning the model, it is used to estimate the additional iron losses due to the stator core fault.

Figure 8 depicts the location of the test coil, the SCF, and the measuring points. It also provides a thermographic image taken during the experiment and the 2D simulation results without/with faulty operation.

4.1. Model Validation

Figure 9(a) shows the current (i) for different faulty conditions ($\delta = 0$; 0.3 and 0.65), where the highly non-linear behavior, due to saturation and hysteresis, becomes visible. The high correlation between experimental and simulation results proves that the parameters of the electromagnetic domain were adjusted properly.

Next, the model of the thermal domain is validated using experimental results. Figure 9(b) shows the temperature for different fault severities in point 1 (upper figure) and point 2 (lower figure). Given that power in the fault region increases with fault severity, the increase of temperature in point 1 is larger than the increase in point 2. Experimental and simulation results show the accuracy of the thermal model.

In addition, Table 2 shows the experimental temperature for point 1 (T_1) and 2 (T_2) for different fault severities at $t = 60$ min. It includes the temperature difference between point 1 and point 2 (ΔT_{12}) which is the only information provided by the thermographic image. Also, the temperature increase in the faulty region respect to the healthy operation (ΔT_{FH}) is

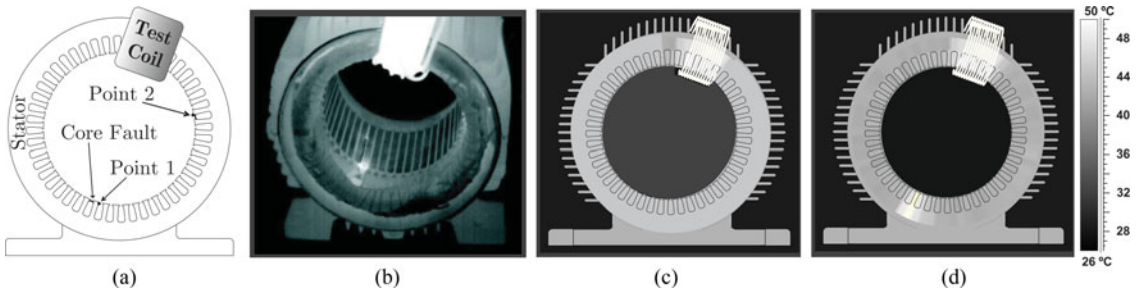

FIGURE 8. (a) Location of the test coil, SCF and measuring points, (b) thermographic image, (c) simulation without fault, and (d) simulation in faulty operation.

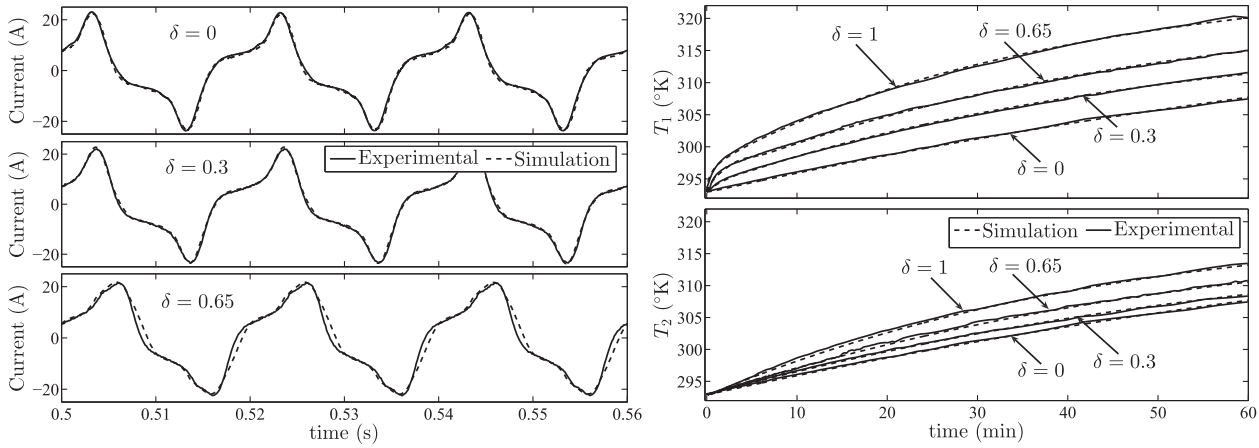

FIGURE 9. (a) Evolution of the test coil current for different fault severities and (b) temperature evolution for point 1 and point 2.

shown in the same table. It is worth mentioning that ΔT_{FH} is impossible to measure experimentally. Nevertheless this temperature would be one of the most important information in order to assess the stator core condition. Note that it is the additional temperature supported by the thermal insulation.

Further discussion is addressed in the final discussion presented in Section 5.

4.2. Additional Iron Losses Evaluation

The instantaneous power is strongly influenced by the saturation and hysteresis effects as can be seen in Figure 10(a). The model is capable to reproduce the instantaneous and mean power for different fault severities.

δ	T_1(°K)	T_2(°K)	ΔT_{12}(°K)	ΔT_{FH}(°K)
0.0	307.4	307.4	0.0	0.0
0.3	311.6	308.4	3.2	4.2
0.65	315.0	310.8	4.2	7.6
1.0	320.1	313.8	6.3	12.7

TABLE 2. Experimental results of temperatures at 60 min. for different fault severities.

Figure 10(b) (upper part) shows that the additional core power (ΔP_{Fe}) obtained with the loop test is similar to the increase of the power losses at no-load operation of the induction machine (ΔP_0) as demonstrated in [27].

The value of ΔP_{Fe} for different severities can be evaluated by simulating the proposed model. Figure 10(b) (lower part) shows experimental and simulated ΔP_{Fe} together with a fitted curve from simulation results.

The fitted curve relates the fault severity with ΔP_{Fe} and can be used to estimate the additional no-load power losses produced by the fault (note that $\Delta P_{Fe} \approx \Delta P_0$). The use of this curve avoids the implementation of complex analytical models for quantifying these losses [28].

5. FINAL DISCUSSION

The proposed model is the result of different contributions in our research group along the last years. On the one hand, the BG representation was used successfully for introducing SCF from its d-q model [12] and faults associated with the windings [26]. In both cases, the impact produced in the thermal domain was studied with a non-validated thermal model. On

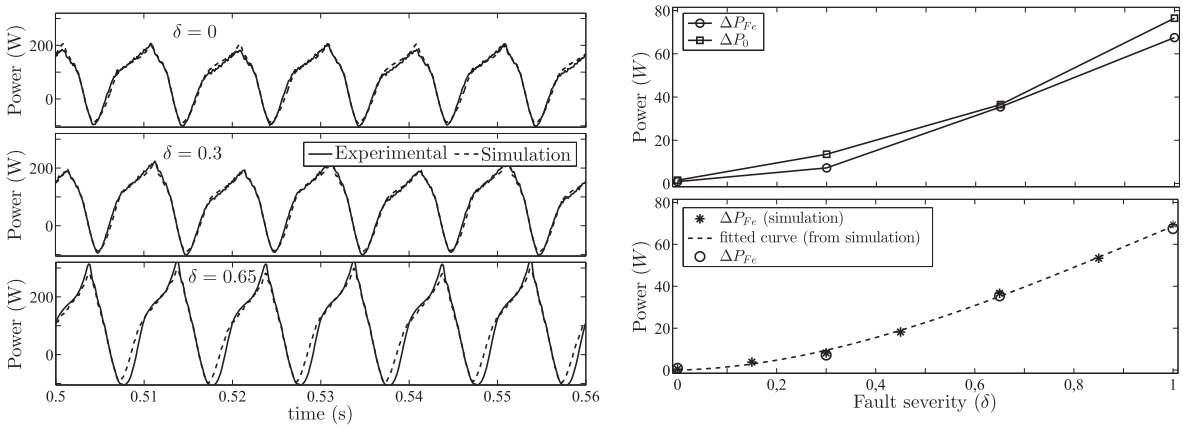

FIGURE 10. (a) Instantaneous power dissipated in the core and (b) increase of P_0 and P_{Fe} for asymmetrical SCF.

the other hand, the experimental method developed for generating a SCF was presented in [27]. The present article exploits the developed BG models adapted to an inter-laminar insulation test. In order to support the presented conclusions, the thermal model was validated experimentally. Thus, the presented model is capable to reproduce accurately the evolution of different variables from the electromagnetic and thermal domains. This feature allows us to evaluate different variables difficult or even impossible to measure such as the magnetic flux confined in the core (ϕ). Note that the stator core inter-laminar insulation test consists in generating ϕ at rated frequency with a density corresponding to 105% of the rated voltage. Therefore, the model is helpful to verify the magnitude of the magnetic flux. Additionally, the proposed model helps to quantify important variables associated with the fault, based on the thermographic image. After the validation process, the model was run multiple times for different fault severities. Table 3 provides essential information from these simulation results. The first column corresponds to ΔT_{12} which is the only information provided by the thermographic image. Using this information, we can estimate the temperature increase in the faulty region (ΔT_{FH}), the additional iron losses (ΔP_0), the impact of ΔP_0 respect to the no-load losses (P_0) and the fault severity.

ΔT_{12}(°K)	ΔT_{FH}(°K)	ΔP_0(W)	$(\frac{\Delta P_0}{P_0})$	δ
1	2.2	4.57	0.61%	0.17
2	4.6	8.18	1.09%	0.24
3	6.9	21.26	2.83%	0.43
4	9.7	35.74	4.77%	0.57
5	13.1	51.25	6.84%	0.71
6	16.4	68.54	9.14%	0.86
7	20.1	85.24	11.39%	0.99

TABLE 3. Temperature related to additional losses and fault severity.

The information presented in this table gives additional information about the increase of the power losses (ΔP_0) and the working temperature of the windings isolation (ΔT_{FH}).

There is a widespread rule of thumb which proposes to repair the SCF when ΔT_{12} is larger than five degrees [29]. This criterion can be redefined based on the information provided in this Table and not only based on ΔT_{12} (the only information obtained from the thermographic image). It worth mentioning that the proposed 2D thermal model assigns a unique temperature in the axial direction (i.e., the axial propagation of heat away from the fault region is not considered). Therefore, the model can be improved by considering two different elements in the faulty region; one accounting for the fault itself and another for the portion of healthy stator core. To accomplish this accurate model, the axial thermal resistivity of the laminated structures must be determined.

The presented model has another drawback related to the temperature rise calculated within the element associated with the fault. This is an average temperature rise, but the local temperature adjacent to the winding is actually higher. The analysis of the previous paragraph is also applicable for solving this drawback. It means that the accuracy of the thermal gradient around the fault region can be increased by refining the meshing. These technical aspects will be analyzed in further works.

6. CONCLUSION

The article presents a multi-domain model of the stator core of an electric machine including inter-lamination short circuits. The model is based on an alternative magnetic equivalent circuit which also incorporates the thermal behavior. The complete model is represented using the Bond Graph

approach that makes apparent the topology of the machine and the energy exchange. The model is obtained intuitively and can reproduce faithfully the dynamics of the system during the fault and the impact on the thermal/magnetic/electric domains.

The proposal provides a theoretical underpinning which support the existing empirical methods used for analyzing the fault severity of a stator core fault. This contribution gives additional information which helps to redefine the criteria about the severity factor and its impact over the machine life and performance.

FUNDING

Consejo Nacional de Investigaciones Científicas y Técnicas (RD N°183/13).

REFERENCES

[1] P. Tavner, "Review of condition monitoring of rotating electrical machines," *Electric Power App., IET*, vol. 2, no. 4, pp. 215–247, 2008.

[2] R. Tallam, S.-B. Lee, G. Stone, G. Kliman, J.-Y. Yoo, T. Habetler, and R. Harley, "A survey of methods for detection of stator-related faults in induction machines," *IEEE Trans. Ind. Appl.*, vol. 43, no. 4, pp. 920–933, 2007.

[3] D. Bertenshaw, A. Smith, C. Ho, T. Chan, and M. Sasic, "Detection of stator core faults in large electrical machines," *Electric Power App., IET*, vol. 6, no. 6, pp. 295–301, 2012.

[4] R. Romary, C. Demian, P. Schlupp, and J.-Y. Roger, "Offline and online methods for stator core fault detection in large generators," *IEEE Trans. Ind. Electron.*, vol. 60, no. 9, pp. 4084–4092, 2013.

[5] S.-K. Kim and J.-K. Seok, "High-frequency signal injection-based rotor bar fault detection of inverter-fed induction motors with closed rotor slots," *IEEE Trans. Ind. Appl.*, vol. 47, no. 4, pp. 1624–1631, 2011.

[6] J. Arellano-Padilla, M. Sumner, and C. Gerada, "Winding condition monitoring scheme for a permanent magnet machine using high-frequency injection," *Electric Power App., IET*, vol. 5, no. 1, pp. 89–99, 2011.

[7] R. Romary, S. Jelassi, and J. F. Brudny, "Stator-interlaminar-fault detection using an external-flux-density sensor," *IEEE Trans. Ind. Electron.*, vol. 57, no. 1, pp. 237–243, 2010.

[8] P. M. de la Barrera and G. Bossio, "Stator core faults detection on induction motor drives using signal injection," in *Diagnostics for Electric Machines, Power Electronics Drives (SDEMPED), 2011 IEEE Int. Symp. on*, 2011, pp. 98–104.

[9] C. Schulz, D. Roger, S. Duchesne, and J.-N. Vincent, "Experimental Characterization of interlamination shorts in transformer cores," *IEEE Trans. Magn.*, vol. 46, no. 2, pp. 614–617, 2010.

[10] J.-P. Bielawski, S. Duchesne, D. Roger, C. Demian, and T. Belgrand, "Contribution to the study of losses generated by interlaminar short-circuits," *IEEE Trans. Magn.*, vol. 48, no. 4, pp. 1397–1400, 2012.

[11] C. Ho, D. Bertenshaw, A. Smith, T. Chan, and M. Sasic, "Three-dimensional finite element analysis of large electrical machine stator core faults," *Electr. Power Appl., IET*, vol. 8, no. 2, pp. 60–7, 2014.

[12] P. M. de la Barrera, L. Silva, C. De Angelo, and G. Bossio, "Multi-domain model of induction motor with stator core faults," in *Industrial Technology (ICIT), 2012 IEEE Int. Conf. on*, 2012, pp. 913–919.

[13] V. Ostović, *Dynamics of Saturated Electric Machines*. New York: Springer-Verlag, 1989.

[14] F. Therrien, M. Chapariha, and J. Jatskevich, "Constant-parameter voltage-behind-reactance induction machine model including main flux saturation," *IEEE Trans. Energy Conversion*, vol. 30, no. 1, pp. 90–102, March 2015.

[15] J. Bacher, F. Waldhart, and A. Muetze, "3-d fem calculation of electromagnetic properties of single-phase induction machines," *IEEE Trans. Energy Convers.*, vol. 30, no. 1, pp. 142–149, March 2015.

[16] F. Impinna, J. Detoni, N. Amati, and A. Tonoli, "Passive magnetic levitation of rotors on axial electrodynamic bearings," *IEEE Trans. Magn.*, vol. 49, no. 1, pp. 599–608, January 2013.

[17] D. C. Hamill, "Lumped equivalent circuits of magnetic components: the gyrator-capacitor approach," *IEEE Trans. Power Electron.*, vol. 8, no. 3, pp. 97–103, April 1993.

[18] D. C. Karnopp, D. L. Margolis, and R. C. Rosenberg, *System Dynamics: Modeling And Simulation of Mechatronic Systems*. USA: Willey InterCiences, 2000.

[19] R. W. Buntenbach, "A generalized circuit model for multi-winding inductive device," *IEEE Trans. Magn.*, vol. 6, no. 1, pp. 65–65, March 1970.

[20] IEEE Std 62.2-2004, *IEEE Guide for Diagnostic Field Testing of Electric Power Apparatus: Electrical Machinery*. IEEE, 2005.

[21] B. Aslan, E. Semail, and J. Legranger, "General analytical model of magnet average eddy-current volume losses for comparison of multiphase pm machines with concentrated winding," *IEEE Trans. Energy Convers.*, vol. 29, no. 1, pp. 72–83, March 2014.

[22] R. A. Naghizadeh, B. Vahidi, and S. H. Hosseinian, "An adaptive approach for simulation of inrush current in three-phase transformers considering hysteresis effects," *Elect. Power Compon. Syst.*, vol. 44, no. 6, pp. 673–682, 2016.

[23] K. Nakamura, S. Hisada, K. Arimatsu, T. Ohinata, K. Sakamoto, and O. Ichinokura, "Iron-loss calculation in a three-phase-laminated-core variable inductor based on reluctance network analysis," *IEEE Trans. Magn.*, vol. 45, no. 10, pp. 4781–4784, October 2009.

[24] N. Leboeuf, T. Boileau, B. Nahid-Mobarakeh, N. Takorabet, F. Meibody-Tabar, and G. Clerc, "Inductance calculations in permanent-magnet motors under fault conditions," *IEEE Trans. Magn.*, vol. 48, no. 10, pp. 2605–2616, October 2012.

[25] M. Bouheraoua, N. Benamrouche, and A. Bousbaine, "A more refined thermal model for a totally enclosed fan-cooled induction motor," *Elect. Power Compon. Syst.*, vol. 40, no. 2, pp. 179–194, 2011.

[26] L. I. Silva, F. Aguilera, P. M. de la Barrera, C. H. De Angelo, and G. O. García, "Multi-domain model for electric traction

drives using bond graphs," *J. Power Electron. (JPE)*, vol. 11, no. 4, pp. 439–448, 2011.

[27] P. M. de la Barrera, M. R. Curti, G. R. Bossio, J. A. Solsona, and G. O. García, "Experimental generation and quantification of stator core faults on induction motors," in *Diagnostics for Electric Machines, Power Electronics Drives (SDEMPED), 2009 IEEE Int. Symp. on*, Cargèse, France, August–September 2009.

[28] D. Kowal, P. Sergeant, L. Dupre, and L. Vandenbossche, "Comparison of iron-loss models for electrical machines, with different frequency domain and time domain methods for excess loss prediction," *IEEE Trans. Magn.*, vol. 51, no. 1, pp. 1–10, January 2015.

[29] *Evaluation tools for electric motor testing: Logic diagrams*. Electric Power Research Institute (EPRI), Palo Alto, CA, Final report, dic. 2001, vol. 1004003.

BIOGRAPHIES

Luis I. Silva received the B.S. degree in Electronics Engineering from the Universidad Nacional de Rosario, Argentina, in 2005; the M.S. in Space Sciences and Technologies from the Lulea Tekniska Universitet, Sweden in 2007; and the Ph.D. of Engineering Sciences from Universidad Nacional de Río Cuarto, Argentina in 2012. From 2013 to 2014, he was postdoctoral fellow at the Universitè de Lille 1, France. Since 2015 he is assistant researcher at the Consejo Nacional de Investigaciones Científicas y Técnicas (CONICET), Argentina. Recent research results are focused on the utilization of graphical modeling techniques in order to evaluate the performance of large-scale electromechanical systems in faulty condition. His research topics are oriented to modeling and simulation applied to electric and hybrid electric vehicles using different graphical descriptions.

Pablo M. de la Barrera received the B.S. and M.S. degrees in electrical engineering from the Universidad Nacional de Río Cuarto, Río Cuarto, in 2003 and 2006, respectively, and the Ph.D. degree in control systems from the Universidad Nacional del Sur, Bahía Blanca, Argentina, in 2009. Since 1998, he has been with the Grupo de Electrónica Aplicada, Universidad Nacional de Río Cuarto. He is also Adjoint Researcher at the Consejo Nacional de Investigaciones Científicas y Técnicas (CONICET), Argentina. He has been an invited researcher in the Institute for Power Electronics and Control of Drives of Technische Universität Darmstadt, Germany during 2009. As well as in the Institute of Electric Power Systems of Otto-von-Guericke-Universität Magdeburg, Germany during Aug.–Oct. 2013, Jun.–Jul. 2014 and Nov.–Dec. 2016. His research interests include modeling, control, and fault diagnosis on electric machines, ac motor drives, electric vehicles, and renewable energy generation.

Roberto Leidhold received the B.S. degree in Electronics Engineering from the Universidad Nacional de Cordoba, Argentina, in 1995; the M.S. degree from the Universidad Nacional de Rio Cuarto, Argentina, in 2000; and the Ph.D. degree from the Universidad Nacional de La Plata, Argentina, in 2003. From 2003 to 2004, he was postdoctoral fellow at the Universidad Nacional de Río Cuarto. From 2005 to 2011, he was with the Technical University of Darmstadt, Germany, first as a Research Scholar of the Alexander von Humboldt Foundation, then as a Research Associate and later as Principal Investigator. Since 2011 he is Professor for electric drive systems at the Otto-von-Guericke-Universität Magdeburg, Germany. His research interests include control of drives, electric machines and renewable energy generation.

Guillermo R. Bossio received the B.S. degree in Electrical Engineering from the Universidad Nacional de Río Cuarto, Argentina, in 1999, and the Ph.D. of Engineering from the Universidad Nacional de La Plata, Argentina, in 2004. Since 1994, he has been with the Grupo de Electrónica Aplicada, Facultad de Ingeniería, Universidad Nacional de Río Cuarto. He is also Independent Researcher at the Consejo Nacional de Investigaciones Científicas y Técnicas (CONICET), Argentina. His research interests include fault diagnosis on electric machines, AC motor drives, electric vehicles, and renewable-energy generation.

Cristian H. De Angelo received the B.S. degree in Electrical Engineering from the Universidad Nacional de Río Cuarto, Argentina, in 1999, and the Ph.D. of Engineering from the Universidad Nacional de La Plata, Argentina, in 2004. In 1994, he joined the Grupo de Electrónica Aplicada, Universidad Nacional de Río Cuarto. He is currently Associate Professor at Universidad Nacional de Río Cuarto and Independent Researcher at Consejo Nacional de Investigaciones Científicas y Técnicas (CONICET), Argentina. His research interests include electric and hybrid vehicles, fault diagnosis on electric machines, electric motors control, and renewable-energy generation.